# Studying Arrhythmic Risk with In-Silico Programmed Ventricular Stimulation and Patient-Specific Computational Models

Thaís de Jesus Soares[1], João Pedro Banhato Pereira[1(✉)], Yan Barbosa Werneck[1], Yuri Rhios Araújo Santos[1], Tiago Dutra Franco[1], Joventino de Oliveira Campos[1], Rafael Sachetto Oliveira[2], Thaiz Ruberti Schmal[1], Thiago Gonçalves Schroder e. Souza[1], Bernardo Martins Rocha[1,2], and Rodrigo Weber dos Santos[1]

[1] Federal University of Juiz de Fora, Juiz de Fora, MG, Brazil
jpbbanhato@gmail.com
[2] Federal University of São João del Rei, São João del Rei, MG, Brazil

**Abstract.** Cardiac arrhythmias can be life-threatening, and early identification of patients at high risk of developing arrhythmias is crucial to implementing preventive measures. Programmed ventricular stimulation (PVS) is a clinical tool to assess arrhythmic risk. In this study, we developed patient-specific computational models using magnetic resonance imaging (MRI) data to evaluate arrhythmic risk through virtual PVS simulations. We applied virtual PVS on a patient with dilated cardiomyopathy and a history of non-sustained ventricular tachycardia. The simulation results revealed the presence of cardiac arrhythmias in the form of spiral waves circulating a fibrotic scar in the patient's heart. These findings, consistent with the patient's medical history, indicate that patient-specific computational models hold great promise as a tool for assessing cardiac arrhythmic risk. The patient-specific computational models have the potential to assist clinicians in identifying high-risk patients and developing personalized treatment plans. By incorporating patient-specific information and simulating various scenarios, computational models can provide valuable insights into the underlying mechanisms of arrhythmia and guide clinical decision-making.

**Keywords:** Computational Modeling of the Heart · Cardiac Arrhythmia

## 1 Introduction

Dilated cardiomyopathy (DCM) is characterized by the ventricular chambers enlargement, often accompanied by impaired myocardial contractile function [7]. Although DCM is typically observed in adults and can be caused by various factors, including infections, myocarditis, autoimmune disorders, and certain medications, it also has a genetic component and may be associated with specific hereditary syndromes [11].

© The Author(s), under exclusive license to Springer Nature Switzerland AG 2023
O. Gervasi et al. (Eds.): ICCSA 2023 Workshops, LNCS 14112, pp. 41–51, 2023.
https://doi.org/10.1007/978-3-031-37129-5_4

In addition to symptoms of heart failure, including reduced ejection fraction, patients with DCM may also present atrial and ventricular arrhythmias and sudden cardiac death (SCD), which can occur at any stage of the disease [7]. As such, it is crucial to identify the etiology and any potential risk factors after a diagnosis of DCM is made.

Currently, implantable cardioverter-defibrillators (ICDs) are recommended for patients with DCM who are at risk of sudden death. However, the decision to use an ICD involves performing complementary tests, some of which may be invasive, such as an electrophysiological study called programmed ventricular stimulation (PVS). This procedure involves the insertion of electrodes into the heart's cavities, which are used to electrically stimulate the heart for varying periods to evaluate the electrical propagation in the cardiac tissue and the induction of arrhythmias.

In this context, virtual models of the heart have emerged as an innovative and increasingly important technology for the non-invasive stratification of SCD risk. Indeed, early research suggests that cardiac computational models are more accurate in predicting SCD risk in patients than classical biomarkers [5].

However, there is still a need for more studies in the literature on non-ischemic patient groups and their correlation with potentially fatal arrhythmias. Thus, the study presented here aimed to create personalized computational models for patients with non-ischemic dilated cardiomyopathy (DCM) and a medical history of non-sustained ventricular tachycardia.

To this end, it is worth noting that magnetic resonance imaging (MRI) data were used to evaluate the patient's arrhythmia risk, and virtual simulations of programmed ventricular stimulation (PVS) were performed.

The results of the implemented simulations revealed the presence of cardiac arrhythmias in the form of spiral waves circulating a fibrotic scar in the patient's heart. Finally, compared to the patient's medical history, these findings were considered consistent.

Finally, it is important to note that the results presented in this work are the first step in an ongoing research project, which aims to help stratify the risk of patients with DCM using computational models. In this sense, the initially obtained results demonstrate the potential of personalized patient computational models to improve risk assessment.

## 2 Materials and Methods

In this section, a clinical description of the patient and the methods used to construct the patient-specific computational model were presented. More specifically, the electrophysiological protocol employed to verify the potential for induction of arrhythmias using a virtual heart of a patient with DCM was presented.

### 2.1 Patient Report

A 61-year-old Caucasian male who smokes presented with symptoms of fatigue, orthopnea, dyspnea NYHA III, and paroxysmal nocturnal dyspnea during his initial visit to the cardiology outpatient clinic at the Federal University of Juiz de Fora's university hospital in January 2023.

The electrocardiogram showed: a heart rate (HR) of 98 bpm, first-degree atrioventricular block, left bundle branch block (LBBB), left atrial enlargement, and left ventricular hypertrophy (LVH). A Doppler echocardiogram revealed dilated cardiomyopathy with an ejection fraction of 19%. The 24-hour Holter evidenced non-sustained ventricular tachycardia. Magnetic resonance imaging showed dilated cardiomyopathy with severe biventricular dysfunction. The exam also showed a left ventricle with greatly increased diameters and cavity volume. Likewise, the right ventricle had increased diameters and cavity volumes. The left atrium was greatly enlarged, and significant mitral regurgitation was also found.

Specific sequences for delayed enhancement showed small regions of linear mesocardial anteroseptal and inferoseptal basal fibrosis and subepicardial fibrosis and inferolateral medial septal fibrosis. This pattern of fibrosis is seen in non-ischemic heart disease.

To treat the symptoms and reduce disease progression Sarcubitril/Valsartan 200mg, Spironolactone 25mg, Bisoprolol 5mg and Dapaglifozin 10mg were prescribed.

Two months after starting the medications, he reports improvement of dyspnea, denies orthopnea, and presents NYHA II. A new ECG showed a positive response to the treatment, with a reduced heart rate of 52 bpm, sinus rhythm, prolonged PR interval, and LBBB.

### 2.2 Magnetic Resonance Imaging (MRI)

Cardiac MRI protocols are designed to evaluate the morphology, functional status, and the presence of myocardial fibrosis in cardiac structures, which may be associated with changes in the cardiac conduction system and possible arrhythmias [1].

Figure 1 presents the image used in the present work, which was acquired using a 1.5 T machine (Avanto, Siemens, Germany) equipped with a dedicated cardiac coil. ECG-gated cine images were obtained in both short-axis and long-axis views, followed by late-enhancement (LGE) imaging 10 min after the injection of a Gadolinium-based contrast agent at a dose of 0.2 mmol/kg, using an inversion recovery T1-weighted gradient-echo sequence. T1-scout was used to determine the appropriate inversion time to null the signal from normal myocardium and regions with LGE were identified and manually segmented.

### 2.3 Computational Mesh

In order to construct a computational mesh for the simulations, the medical image (Fig. 1) was segmented using Seg3D software [2]. Figure 2a presents the

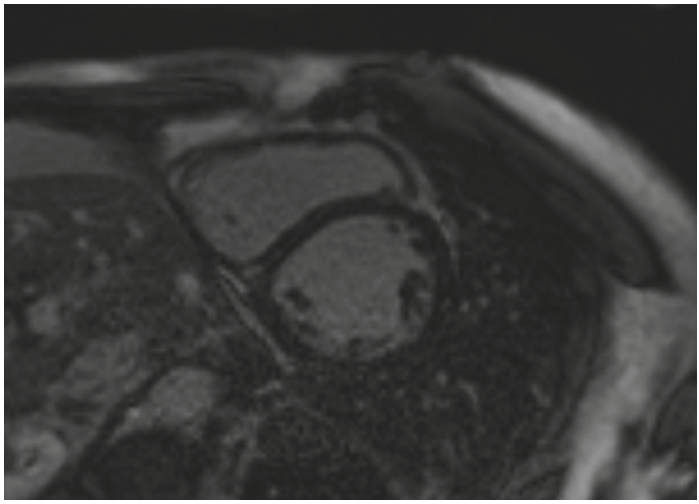

**Fig. 1.** Cardiac MRI image from the patient used to generate the computational domain for the simulations of the present study.

segmentation process, where the epicardium and endocardium borders of the ventricles are marked with green lines. The regions with fibrosis are also marked in red on the image.

The segmented regions were exported, and the Gmsh software [4] was used to generate a discretization for the domain, resulting in the mesh presented in Fig. 2b. In addition, each element was marked to indicate the presence or absence of fibrosis.

Finally, a script was used to convert the Gmsh mesh to the format used in MonoAlg3D [8], which was the chosen software to carry out the computational simulations.

### 2.4 Mathematical Model

To model the electrical activity of the patient's heart, the monodomain equation [9] was used. The monodomain equation describes the propagation of action potential in cardiac tissue via a rection-diffusion partial differential equation. To describe the action potential generation at the myocyte level, the ten-Tusscher cell model [10] was used, which consists of 19 ordinary differential equations. A complete description of the ten-Tusscher model is available in [10].

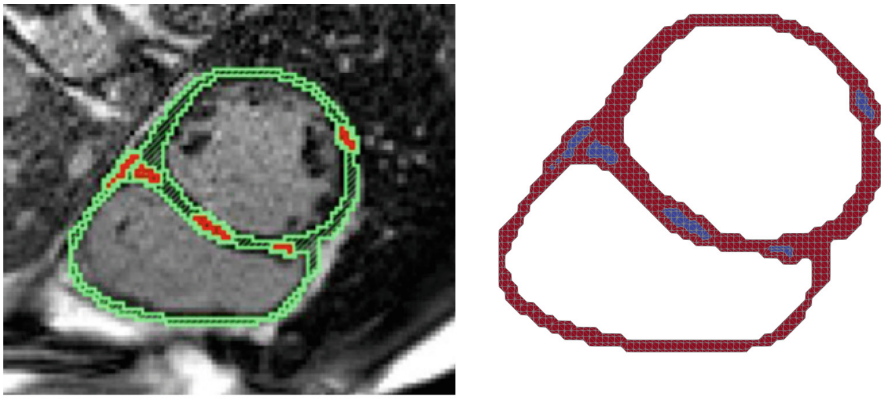

(a) Segmented region. (b) Computational mesh.

**Fig. 2.** Image processing to generate the computational mesh for the simulations. (a) the segmented region from a short-axis MRI image of the patient's heart including healthy tissue (in green) and fibrotic regions (in red); (b) computational mesh representation of the segmented domain. (Color figure online)

The model consists of a reaction-diffusion partial differential equation coupled to a system of ordinary differential equations, which is given by:

$$\chi\left(C_m\frac{\partial V}{\partial t}\right)+(I_{ion}+I_s)=\nabla\cdot(\sigma\nabla V), \tag{1}$$

$$I_{ion}=g(V,\eta,t), \tag{2}$$

$$\frac{\partial\eta}{\partial t}=f(V,\eta,t), \tag{3}$$

where $\chi$ is the surface-to-volume ratio of cells ($\mathrm{mm}^{-1}$), $C_m$ is the specific membrane capacitance per unit area ($\mu\mathrm{F\ mm}^{-2}$), $V$ is the transmembrane potential (mV), $\eta$ is a vector of state variables, $I_{ion}$ is the transmembrane current density ($\mu\mathrm{A\ mm}^{-2}$) representing the sum of all transmembrane ionic currents and $I_s$ is the density of an imposed stimulus current, while $\sigma$ is the electrical conductivity ($\mathrm{mS\ mm}^{-1}$).

The electrical conductivity was considered isotropic and heterogeneous, with a reduced conductivity value used in fibrotic regions. Besides, the no-flux boundary condition is applied in the entire boundary to represent that the tissue is electrically insulated.

The mathematical model was solved using the finite volume method on the discretized domain, which consists of approximately 70000 volumes of the same size ($0.2 \times 0.2 \times 0.2\ \mathrm{mm}^3$). To obtain the transmembrane potential for each computational cell, the simulation of the monodomain equation requires the solution of a system of linear equations for each time step, which is solved using

the conjugate gradient iterative method. This numerical solution is implemented in the MonoALG3d simulator [8], used in the present work.

**Table 1.** Results of the simulated study protocol. The first column identifies the stimulus, and the second column shows the number of applications of each stimulus. The third and fourth columns show the start and end times at which it was analyzed. The fifth column shows the interval between the current stimulus and the previous one. The last three columns show the classification for each simulation.

| Stimulus (S) | Applications | Start time | End time | Interval | Reentry | Block | Normal |
|---|---|---|---|---|---|---|---|
| 1 | 8 | 0 | 4200 | 600 | | | X |
| 2 | 1 | 4580 | 6000 | 380 | | X | |
| 2 | 1 | 4590 | 6000 | 390 | X | | |
| 3 | 1 | 4970 | 7000 | 380 | | | X |
| 3 | 1 | 4960 | 7000 | 370 | | | X |
| 3 | 1 | 4950 | 7000 | 360 | | | X |
| 3 | 1 | 4940 | 7000 | 350 | | | X |
| 3 | 1 | 4930 | 7000 | 340 | | | X |
| 3 | 1 | 4920 | 7000 | 330 | | | X |
| 3 | 1 | 4910 | 7000 | 320 | | | X |
| 3 | 1 | 4900 | 7000 | 310 | | | X |
| 3 | 1 | 4890 | 7000 | 300 | X | | |
| 3 | 1 | 4880 | 7000 | 290 | X | | |
| 3 | 1 | 4870 | 7000 | 280 | X | | |
| 3 | 1 | 4860 | 7000 | 270 | | X | |
| 4 | 1 | 5250 | 7000 | 380 | X | | |
| 4 | 1 | 5240 | 7000 | 370 | X | | |
| 4 | 1 | 5230 | 7000 | 360 | X | | |
| 4 | 1 | 5220 | 7000 | 350 | X | | |
| 4 | 1 | 5210 | 7000 | 340 | X | | |
| 4 | 1 | 5200 | 7000 | 330 | | X | |

### 2.5 Simulating Programmed Ventricular Stimulation

Programmed ventricular stimulation was performed in-silico using a simple sequential protocol, as previously described [3]. The protocol consists of the extra stimulus mode, using an 8-beat drive train at the outflow tract at the ventricular-paced cycle length of 600 ms. The first extra stimulus (S2) is delivered initially with an S1-S2 interval of 380 ms and decremented in 10 ms steps until the effective refractory period (ERP) or when 200 ms is reached. S2 is then moved out 10 ms, and S3 is introduced with an initial S2-S3 interval of 380 ms, decremented in a similar fashion. S4 was delivered in a similar pattern.

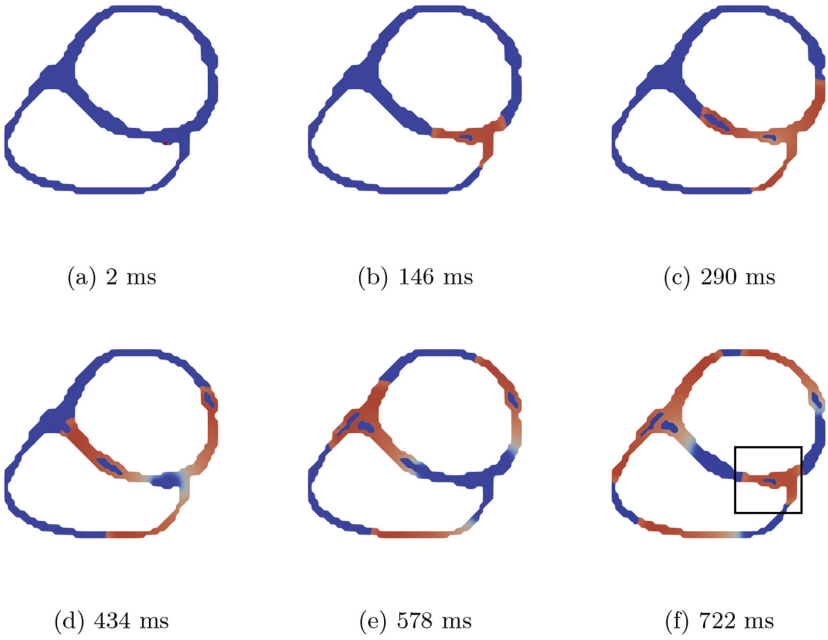

(a) 2 ms (b) 146 ms (c) 290 ms

(d) 434 ms (e) 578 ms (f) 722 ms

**Fig. 3.** Electrical propagation of Stimulus 1 (S1) at different time steps, showing a normal propagation. (a) the stimulus has been applied, (b) the stimulus propagates regularly in all directions. In (c), (d), and (e), the wave continues to propagate stimulating the whole tissue. In (f) we have the beginning of the propagation of the second stimulus in the S1 protocol. Transmembrane potential ranges from -80 mV (blue color) to 40 mV (red color). The black square shows the region around the stimulus in which we'll focus our analysis. (Color figure online)

### 2.6 Computational Experiment

Computational simulations were performed to reproduce the Programmed Ventricular Stimulation protocol using the mesh presented in Fig. 2b. The conductivity is considered isotropic with $\sigma = 0.00002$ mS mm$^{-1}$ at healthy volumes and $\sigma = 2.5 \cdot 10^{-7}$ mS mm$^{-1}$ for volume with fibrosis. Furthermore, to simulate the use of a catheter during the electrophysiological study protocol, a stimulus with a duration of 2 ms and amplitude of -38 $\mu$A/$\mu$m$^2$ was used. The stimulated region was a 2 mm square near the right ventricular outflow tract (RVOT). This region was chosen because, according to literature studies [6], it is the most pro-arrhythmic ectopic location.

During the protocol simulation, it is worth noting that three possible outcomes were considered: normal propagation, block, or arrhythmia. In normal propagation, the stimulus is able to electrically activate neighboring cells in the

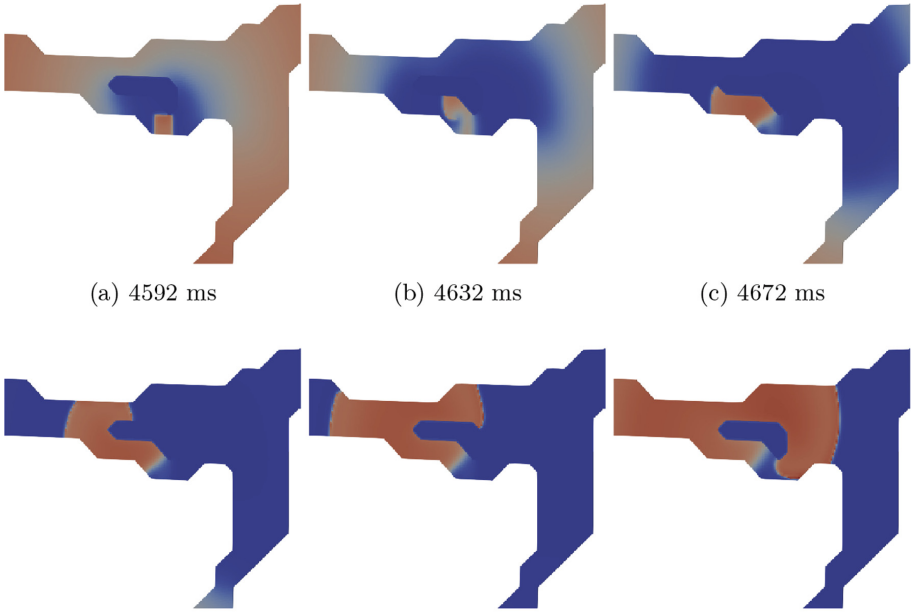

(a) 4592 ms (b) 4632 ms (c) 4672 ms

(d) 4712 ms (e) 4752 ms (f) 4792 ms

**Fig. 4.** Propagation of the (S2) stimulus with an interval of 390 ms at different time steps. (a) the beginning of propagation right after a stimulus. (b) and (c) after 40–80ms, the wave propagates to the right but not the left, causing the beginning of the spiral formation. (d) 120 ms after the stimulus, the wave now starts propagating to the left. (e) and (f) generation of a reentry spiral in the zoomed region. Transmembrane potential ranges from -80 mV (blue color) to 40 mV (red color).

region where it was applied. Moreover, the stimulated cells return to their initial conditions after surpassing their refractory periods.

On the other hand, in block, the stimulus is applied to a region that is still in its refractory period and therefore becomes unable to stimulate the cells in its vicinity.

Finally, in arrhythmia or reentry, the cells within a region are able to self-stimulate, either sustainably or unsustainably. In the computational model, this condition is represented by the generation of a spiral wave of electrical excitation.

## 3 Results

This section presents the results obtained with the simulation of the electrophysiological study protocol. With a fixed initial stimulus (S1) at the start, various simulations were run for each subsequent stimulus (S2, S3, S4), in order to find

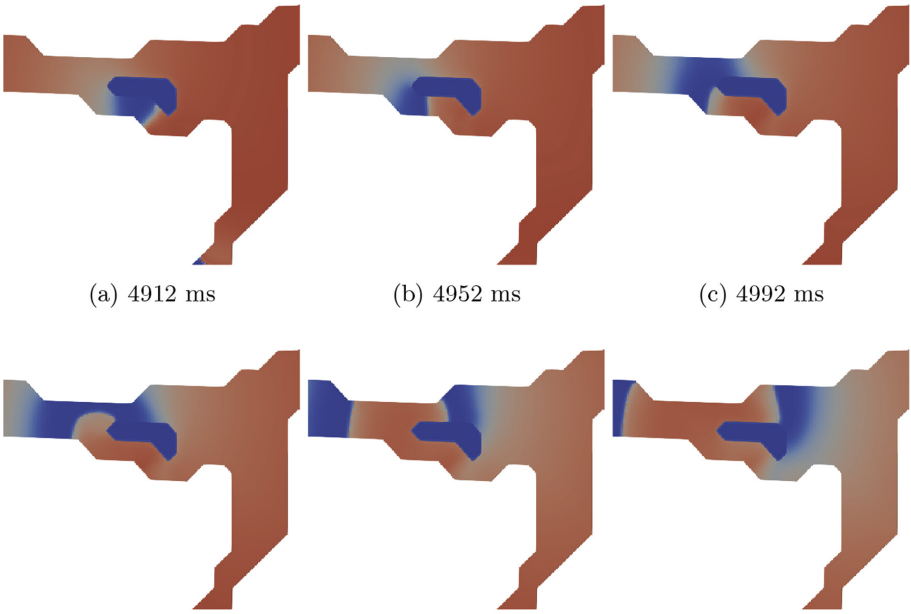


**Fig. 5.** Propagation of Stimulus S3 with an interval of 300 ms at different time steps, showing a spiral formation. (a) 2 ms after the stimulus shows that right after it, the region around the stimulus is still depolarized, with a small portion of repolarized tissue to the left. (b) the S3 wave propagating to this region of repolarized tissue. In (c) and (d) the regions to the right and above the fibrosis region start the repolarization while in (e) the wave starts propagating to the right. (f) Formation of a reentry spiral, which will cause 4 arrhythmia cycles. Transmembrane potential ranges from -80 mV (blue color) to 40 mV (red color). (Color figure online)

the blockage time for each stimulus and advance to the next step of the protocol. Each run was classified as block, normal propagation, or reentry and the results are summarized in Table 1.

As expected, it was observed that during the initial 8-beat drive train (S1) application, all stimuli resulted in normal propagation to the whole tissue without generating a spiral or block, as presented in Fig. 3.

Then, the second stimulus (S2) was applied. At this stage, it is important to highlight two different situations. S2 when applied with an interval of 380 ms blocks. However, when we moved to the S3 step, S2 is applied again with an interval of 10 ms greater than previously, which caused reentry. The observed reentry is in the pattern of a small spiral around one of the fibrotic regions, as presented in Fig. 4.

For the third stimulus (S3), reentries were observed in intervals from 300 ms to 280 ms. Figure 5 shows an unsustained spiral around one of the fibrotic regions after the S3 stimulus. The spiral re-excited the tissue four times (4 waves) before self-termination. At the interval of 270 ms, S3 blocks.

For the fourth stimulus (S4), similar unsustained reentries were observed for stimulus intervals between 380 ms and 340 ms S4 propagation blocks at the interval of 330 ms.

## 4 Conclusion

This work presented computational simulations of the propagation of electric waves in cardiac tissue using a simulator based on the Monodomain mathematical model. The simulations using patient-specific geometry were performed to reproduce an invasive procedure called electrophysiological study, which is normally used to investigate the risks of cardiac arrhythmia in patients with heart disease. A virtual programmed ventricular stimulation was performed and identified non-sustained cardiac arrhythmias in the form of spiral waves that circulated one of the patient's fibrotic scar. The spiral wave arises due to the interplay of tissue heterogeneity, i.e., fibrotic regions captured by the cardiac MRI exam of the patient, and electrophysiology features, reproduced by the computational models.

The cardiac arrhythmias found using the patient-specific model are consistent with the patient's history of non-sustained ventricular tachycardia, as described in Subsect. 2.1. It is crucial to emphasize that the modeling and results outlined in this work are just the first steps of a broader ongoing research project. The ultimate goal is to enhance our understanding of the physiopathological mechanisms responsible for generating cardiac arrhythmias in patients with heart diseases. This research will help us identify new therapeutic targets and enhance clinical practice in cardiology, thereby improving patient outcomes.

**Acknowledgements.** This work was supported by NVIDIA (project "Patient-specific models of the heart for precision medicine", NVIDIA Academic Hardware Grant Program), by the Federal University of Juiz de Fora (UFJF), through a scholarship from the "Coordenação de Aperfeiçoamento de Emprego de Ensino Superior" (CAPES) - Brazil - Finance Code 001, by the National Council for Scientific and Technological Development (CNPq), by the "Empresa Brasileira de Serviços Hospitalares" (Ebserh) grant numbers 423278/2021-5, 310722/2021-7, and 315267/2020-8, and by the Minas Gerais State Research Support Foundation (FAPEMIG) - Brazil TEC APQ 01340-18 and APQ 00748-18.

## References


1. Balaban, G., et al.: Late-gadolinium enhancement interface area and electrophysiological simulations predict arrhythmic events in patients with nonischemic dilated cardiomyopathy. Clin. Electrophysiol. **7**(2), 238–249 (2021)
2. CIBC: seg3D: Volumetric Image Segmentation and Visualization. Scientific Computing and Imaging Institute (SCI) (2016). http://www.seg3d.org
3. Fisher, J.D., Kim, S.G., Ferrick, K.J., Roth, J.A.: Programmed ventricular stimulation using tandem versus simple sequential protocols. Pacing Clin. Electrophysiol. **17**(3), 286–294 (1994)
4. Geuzaine, C., Remacle, J.F.: GMSH: a 3-d finite element mesh generator with built-in pre-and post-processing facilities. Int. J. Numer. Meth. Eng. **79**(11), 1309–1331 (2009)
5. Huynh, K.: Arrhythmia risk stratification using virtual heart models. Nat. Rev. Cardiol. **13**(7), 381–381 (2016)
6. Martinez-Navarro, H., Zhou, X., Bueno-Orovio, A., Rodriguez, B.: Electrophysiological and anatomical factors determine arrhythmic risk in acute myocardial ischaemia and its modulation by sodium current availability. Interface Focus **11**(1), 20190124 (2021)
7. Report of the WHO/ISCF task force: On the definition and classification of cardiomyopathies. Br. Heart J. **44**, 672–673 (1980)
8. Sachetto Oliveira, R., et al.: Performance evaluation of GPU parallelization, space-time adaptive algorithms, and their combination for simulating cardiac electrophysiology. Int. J. Numer. Methods Biomed. Eng. **34**(2), e2913 (2018)
9. Sundnes, J., Lines, G.T., Cai, X., Nielsen, B.F., Mardal, K.A., Tveito, A.: Computing the Electrical Activity in the Heart, vol. 1. Springer Science & Business Media, Heidelberg (2007). https://doi.org/10.1007/3-540-33437-8
10. Ten Tusscher, K.H., Panfilov, A.V.: Alternans and spiral breakup in a human ventricular tissue model. Am. J. Physiol.-Heart Circ. Physiol. **291**(3), H1088–H1100 (2006)
11. Walter, H.A., Beverly, H.L.: The challenge of cardiomyopathy. J. Am. Coll. Cardiol. **13**(6), 1219–1239 (1989)